Process Development for Printing Copper Conductible Ink on Flexible Substrates using Aerosol Jet Printing Technology

Pradeep Lall
Auburn University
NSF-CAVE3 Electronics Research Center,
Department of Mechanical Engineering,
Auburn AL 36849
Email – lall@auburn.edu

Ved Soni
Auburn University
NSF-CAVE3 Electronics Research Center,
Department of Mechanical Engineering,
Auburn, AL 36849

Curtis Hill
Jacobs Space Exploration Group | Quantitech
NASA Marshall Space Flight Center
Huntsville, AL

***Abstract* - Rise in demand for wearable consumer electronics products has given an impetus to the development of flexible electronics technology encompassing flexible substrates and compatible circuitry. Also, additive manufacturing of flexible electronics is emerging rapidly via several techniques such as Inkjet and Aerosol Jet Printing (AJP). The basic component of all flexible circuits to be printed by these technologies is conductible ink, which is generally silver ink. Few studies exist on the printing of copper conductible ink and not many copper ink formulations are available in the market as that of silver inks. This study aims to develop a process development study for deposition of copper conductible lines on flexible substrates using the aerosol jet printing technology. The process development study includes investigation of photosintering parameters for obtaining desirable electrical resistance and shear load to failure values for the printed line. Different pre-drying techniques such as oven pre-drying and platen pre-drying have been used for improving the electrical and mechanical properties of the conductive traces. Techniques such as optical microscopy and white light interferometry have been used for the characterization of print quality of the conductible lines.**

Keywords - aerosol jet printing, copper conductible ink, process development, electrical resistance, shear load to failure

I. Introduction

The rising demand for flexible consumer electronics and the ongoing trend of miniaturization and lightweight design are two of the main factors which have provided impetus to the technological progress in manufacturing additively printed electronics. These technologies are primarily used for fabrication of sensors, optoelectronics and batteries, with several end-user industries such as consumer electronics, automotive, healthcare, and transportation [1]. Owing to such high-value application areas, the research in the field of printed electronics has led to the development of many flow-based, droplet-based, energy beam-based and tip based 'direct-write' technologies, which rely on distinct scientific principles for depositing printed material onto a substrate [2].

Aerosol Jet Printing (AJP) is a droplet-based, non-contact direct-write technology used for the additive printing of electronics. To date, AJP has been used in the fabrication of various circuit components using a variety of materials on conformal as well as planar substrates with different textures. Material deposition using aerosol jet printing begins with aerosolizing of the material into 2-5 µm diameter droplets [3] using either pneumatic or ultrasonic atomization. These two atomization processes allow the AJP machine to work with inks and dielectrics with a wide range of viscosities from 1 to 1000 cP [3]. Also, AJP facilitates in-situ adjustment of the material deposition rate which in turn allows control over the line feature sizes. To date, the demonstrated feature sizes range from 10 µm to several millimeters [4]. Owing to this repertoire of technological prowess, the AJP process has been used in the fabrication of various electronic circuit components such as conductive lines, passive components, interconnects, etc.

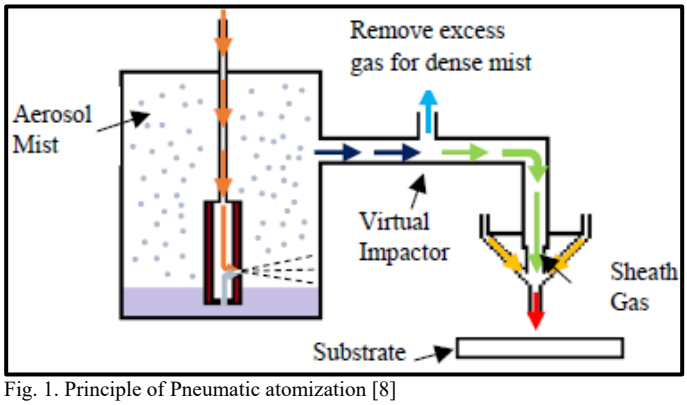

Fig. 1. Principle of Pneumatic atomization [8]

The most basic application of AJP being the printing of conductible lines, the earliest studies in this field were done on the development of process windows for printing process parameters for various conductible inks. As described previously, AJP involves many process parameters and their optimization is a tedious process entailing the consideration of electrical and mechanical characteristics (electrical resistance, adhesion, etc.) of printed lines apart from the print quality (line

consistency, overspray, etc.). Verheecke [5] and Mahajan [6] performed extensive process window development studies for conductible lines considering the electrical characteristics and print quality of the line. Secor [7] performed an analytical investigation of AJP using simplistic physical models and graphed the effect of various process parameters such as carrier gas flow rate, sheath flow rate and nozzle diameter on the line width and its profile thereby providing guidelines for printing of conductible inks. Lall [8] performed a line consistency study for various geometries of printed conductive traces. Lall [9] investigated the effect of sintering conditions, namely sintering time and sintering temperature on the electrical and mechanical properties of the conductible line. Furthermore, they also performed a print consistency study where the variation in physical, mechanical, and electrical characteristics of the line when printing for an extended time period of ten hours was observed.

The literature on printing of pure copper inks is not very rich. Instead, there are studies exhibiting the printing of copper oxide nanoparticle ink and its further sintering via photonic methods to form copper. Among photonic sintering methods, laser sintering Rahman [10] and flash white light sintering are the popular ones. Rager [11] used pulse thermal processing for sintering CuO nanoinks and achieved print with resistivity of 10 μΩ.cm within less than a second of pulse time. Kang [12] performed direct intense pulsed light sintering of inkjet printed CuO layers and obtained a resistivity of 5.54 μΩ.cm. Chung [13] used intense pulsed light sintering for printed copper nanoparticles and achieved a lowest resistivity of 10 μΩ.cm. Hwang [14] combined flash white light photonic sintering with deep-UV and near infrared irradiation to produce a conductive copper nano-ink film having a resistivity of 7.62 μΩ.cm.

This work focuses on process development for printing conductible lines and circuits using copper ink on polyimide substrate. The process development consists of several sub-studies such as study of the effect of photosintering parameters, effect of oven and platen pre-drying on the electrical and mechanical properties of the printed conductible lines. The results generated have been supported with optical microscopy and white light interferometry surface plots as well.

II. Experimental Methodology

A. Test Vehicle

The conductive copper ink chosen has 60% copper solid content by weight and has a viscosity of 30 cP (see TABLE I). The pneumatic atomizer of AJP has been used for printing the copper ink.

TABLE I: Properties of Conductible Copper Ink Used as a Test Vehicle

Ink Properties	Value
Solid Content (Weight %)	60 %
Viscosity	30 – 40 cP
Particle Size	90 nm
Bulk Resistivity	3.4 – 6.8 μΩ

The printing process and parameters selected for printing have been pre-determined using the process detailed in [8]. Throughout the study, the printing was conducted on a polyimide substrate which was cleaned with a spray of isopropyl alcohol (IPA). For each printing run, the vial was loaded with a small amount of conductible ink and was maintained at the ambient temperature. Also, the substrate was maintained at a temperature of 30 °C using the platen heater. A 300 μm nozzle was used for printing the ink which was maintained at a standoff height of 2 mm from the substrate. The stage speed used was set at 4 mm/s. The pneumatic atomizer mass flow control rate (PAMFC) was set to 400 standard cubic centimeters per minute (sccm) and the exhaust gas flow rate was varied so that the difference between the two lied in the range as shows in TABLE II. The sheath (carrier) gas flow rate was also set to a fixed value of 50 sccm.

TABLE II: Aerosol Jet Process Parameters Used for Ink Printing

Parameter	Value
Nozzle Diameter	300 μm
Standoff Height	2 mm
Ink Temperature	Ambient (25°C)
Platen Temperature	30°C
Pneumatic Atomizer Mass Flow Rate (PAMFC)	400 sccm
Δ (Pneumatic – Exhaust) Mass Flow Rate	15 – 40 sccm
Sheath Gas Flow Rate	50 sccm
Stage Speed	4 mm/s

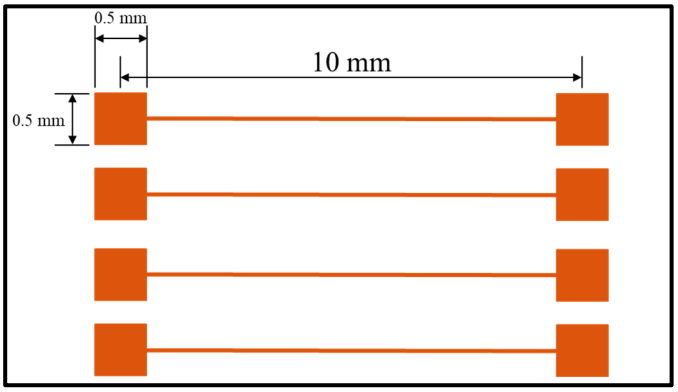

Fig. 2. Schematic of the printed conductive traces used for all the investigations in the present study

B. Test Matrix

This section presents the different test matrices for the investigations performed in this work.

TABLE III: Test Matrix of Operating Voltages for Line Photosintering Study

Sr. No.	Voltage (V)	Energy (J)	No. of bursts	Burst frequency (Hz)
1	1900	700	5	0.17
2	2000	700	5	0.17

Sr. No.	Voltage (V)	Energy (J)	No. of bursts	Burst frequency (Hz)
3	2100	700	5	0.17
4	2200	700	5	0.17
5	2300	700	5	0.17
6	2400	700	5	0.17

The photonic sintering process used for sintering the printed samples consists of multiple process parameters which vary over a wide range. Following are the parameters varied for examining the effect of photo-sintering conditions on the electrical and mechanical properties of the printed line: operating voltage (V), flash energy (J), no. of bursts, and burst frequency (Hz). The no. of bursts represents the number of flashes of a single pulse which the machine performs on the sample. And finally, the burst frequency represents the amount of flashes the machine performs in one second. Thus, a multitude of sintering conditions were examined by studying the effect of each parameter on the electrical resistivity and shear load to failure of the printed sample. TABLE III, TABLE IV, TABLE V, and TABLE VI list the various combinations of sintering parameters investigated for the photonic sintering study.

TABLE IV: TEST MATRIX OF FLASH ENERGIES FOR LINE PHOTOSINTERING STUDY

Sr. No.	Voltage (V)	Energy (J)	No. of bursts	Burst frequency (Hz)
1	2100	300	5	0.17
2	2100	700	5	0.17
3	2100	1000	5	0.17
4	2100	1267	5	0.17

TABLE V: TEST MATRIX OF NO. OF PHOTO-SINTERING FLASHES FOR PHOTOSINTERING STUDY

Sr. No.	Voltage (V)	Energy (J)	No. of bursts	Burst frequency (Hz)
1	2100	700	1	0.17
2	2100	700	3	0.17
3	2100	700	5	0.17
4	2100	700	10	0.17

TABLE VI: TEST MATRIX OF PHOTO-SINTERING FLASH FREQUENCIES FOR PHOTOSINTERING STUDY

Sr. No.	Voltage (V)	Energy (J)	No. of bursts	Burst frequency (Hz)
1	2100	700	5	0.5
2	2100	700	5	0.25
3	2100	700	5	0.17
4	2100	700	5	0.125

Apart from the photosintering study, investigations were conducting the pre-drying of printed samples prior to photosintering so as to effectively evaporate the ink solvent present in the printed lines. Two methods of pre-drying were used: oven pre-drying and platen pre-drying. In both the methods, the printed samples were pre-dried at different temperatures and for different time intervals, which are listed in TABLE VII. For the oven pre-drying case, the samples were affixed to a glass sheet and were then placed in the oven for sintering. Whereas for the platen pre-drying scenario, the samples were printed on a pre-heated platen itself and were kept on the platen up to the specified time duration.

TABLE VII: TEMPERATURE AND TIME COMBINATIONS USED FOR PRE-DRYING TESTS

Sr. No.	Pre-Drying Temperature (°C)	Pre-Drying Time (min)
1	50	5
2		15
3		25
4	65	5
5		15
6		25
7	80	5
8		15
9		25

III. RESULTS AND DISCUSSION

This section details the results of the various investigations described in the test matrix, namely, the photosintering study and the oven and platen pre-drying study. Four lines were printed per sample so as to ensure the statistical significance of measured parameters. For shear load to failure testing, multiple readings were recorded and the average of those readings has been plotted along with the standard deviation as the error bars.

A. Effect of photosintering parameters on the electrical and mechanical properties of printed conductible lines

As mentioned in the earlier section, following were the photo-sintering parameters varied for examining their effect on the line electrical and mechanical properties: the operating voltage (kV), the flash energy (J), the burst period (ms) and the number of bursts. For the entire photo-sintering investigation a line with length 10 mm was printed for evaluation of its electrical and mechanical properties. Also, for each photo-sintering condition, four lines were printed for ensuring the statistical significance of the properties evaluated.

Fig. 3 shows the plot of photosintering power (kW) v/s time for voltages ranging from 1900 V to 2400 V. For all these pulses the flash energy is constant at 700 J. Due to the constant energy condition, the pulse with the lowest voltage i.e. 1900 V lasts for a longer duration of time whereas the pulse with the higher voltage i.e. 2400 V lasts for a shorter duration. Also, since the area under the power v/s time curve indicates the pulse energy, it can be observed that the area under all these curves is the same. Fig. 4 and Fig. 5 show the plots of electrical resistivity and shear load to failure for different photosintering voltages. With an increase in the operating voltage, a mild increase in electrical resistivity is seen up till 2300 V. The samples sintered at 2400 V reported an open circuit and hence do not have a

resistivity value associated with them. The shear load to failure increases marginally with an increase in the operating voltage up to 2200 V and again decreases.

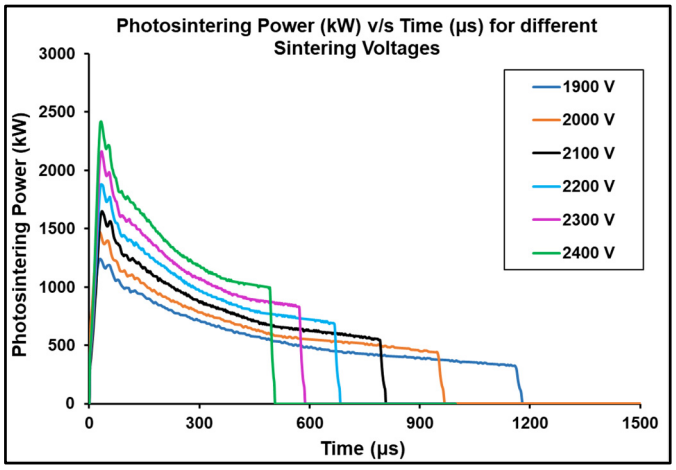

Fig. 3. Photosintering power v/s time for different photosintering voltages

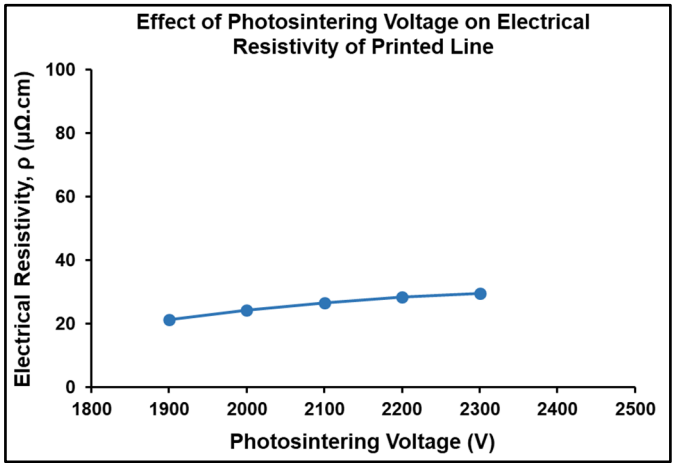

Fig. 4. Effect of photosintering voltage on electrical resistivity of printed conductive lines

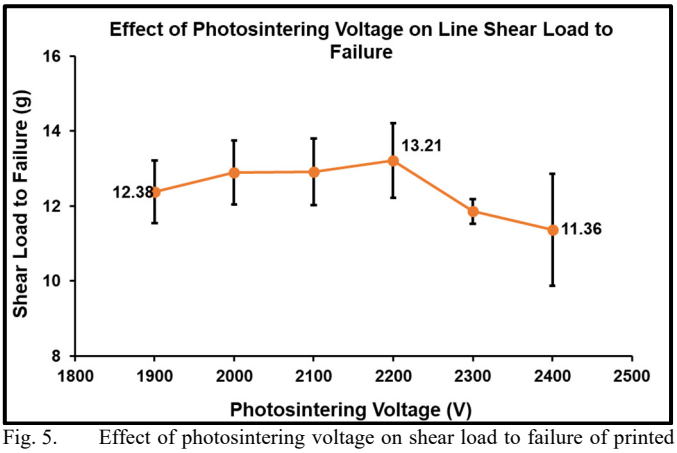

Fig. 5. Effect of photosintering voltage on shear load to failure of printed conductive lines

Fig. 6 depicts the microscopic optical images of the conductive traces sintered with different voltages. It can be seen that with increase in the operative voltage, the line becomes visibly brighter as the copper nanoparticles are sintered well. Furthermore Fig. 7 shows the surface profile of the sintered traces scanned using white light interferometry. The trace sintered under 1900 V is observed to have to small cracks along its lengths. Investigation of the cross-sectional area at the crack location shows that a burst akin to a popcorn failure has occurred in the line which has forced the material outwards. This can occur due to ink solvent still being present in the conductive trace during sintering. As the solvent evaporates due to the high photosintering temperatures, it escapes through the top of the line generating a popcorn crack site in the conductible line. As the photosintering voltage is increased, the number of such cracks increase. In Fig. 7 (F), the entire material of the line is popcorned outwards due to the high energy corresponding to 2400 V. The optical image for this case (Fig. 6 (E)) also shows a removal of sintered copper from the line exposing the PI substrate underneath.

This nature of the sintering can explain the increase in resistivity with increase in voltage, due to the material being thrown outwards in a popcorned manner, and furthermore it would also explain the open circuit observed for 2400 V. This also explains the shear load to failure trend observed. As the operating voltage increases, the line gets sintered well which leads to an increase in the shear load to failure. However, as the voltage increases beyond 2200 V, excessive popcorning occurs due to high voltage and due to the material being forced outwards, the shear load to failure decreases. Fig. 8 shows the plot of photosintering power (kW) v/s time for different flash energies ranging from 300 J to 1267 J. For all these pulses the operating voltage is constant at 2100 V. Due to the constant voltage condition, the pulse with the lowest flash energy i.e. 300 J lasts for the shortest time duration whereas the pulse with the highest energy i.e. 1267 J lasts for the longest duration. Also, since all the conditions are performed at the same voltage, the peak power for all the cases is the same.

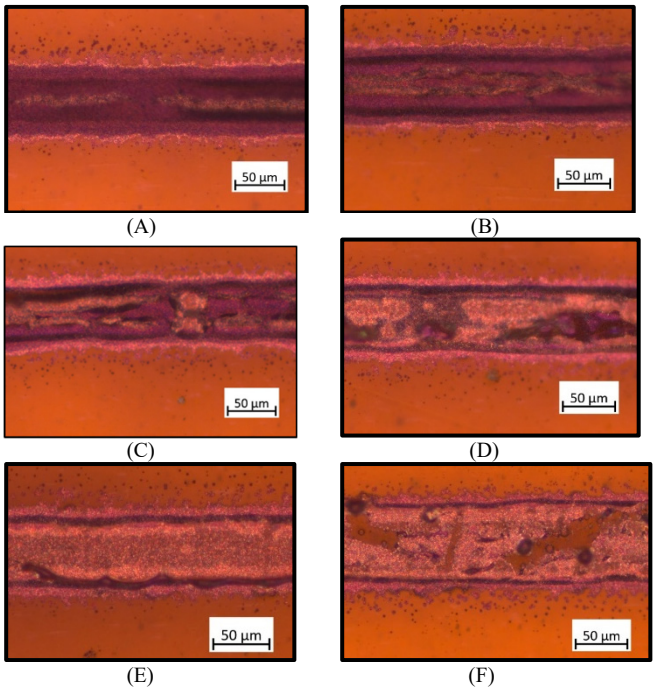

Fig. 6. Optical images of printed conductible lines sintered with different photosintering voltages (A) 1900 V, (B) 2000 V, (C) 2100 V, (D) 2200 V, (E) 2300 V, and (F) 2400 V

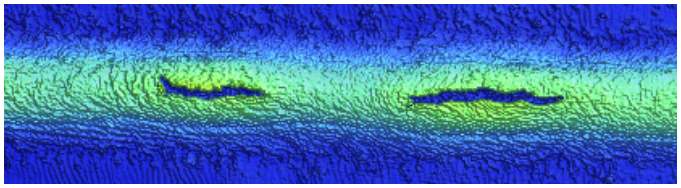

(A)

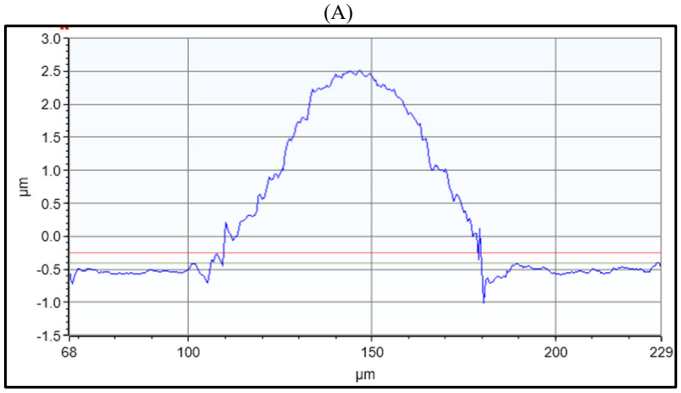

(B)

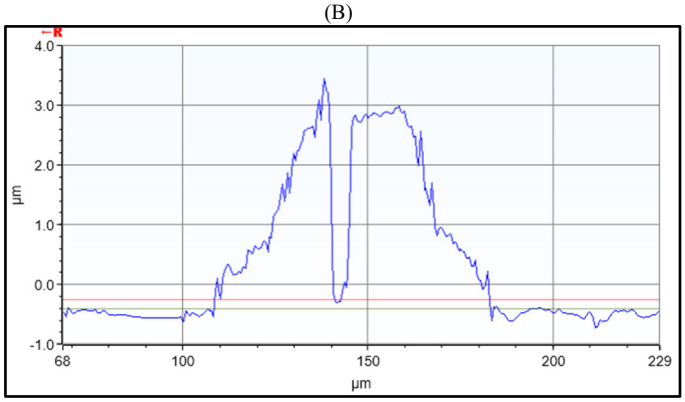

(C)

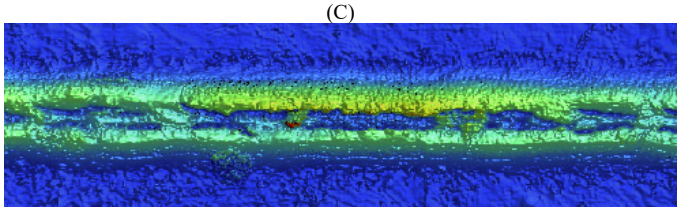

(D)

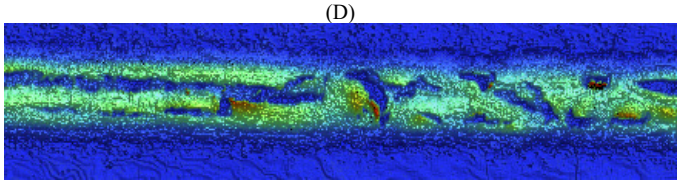

(E)

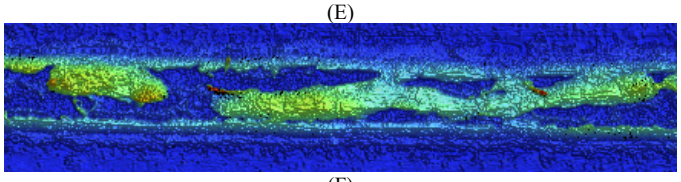

(F)

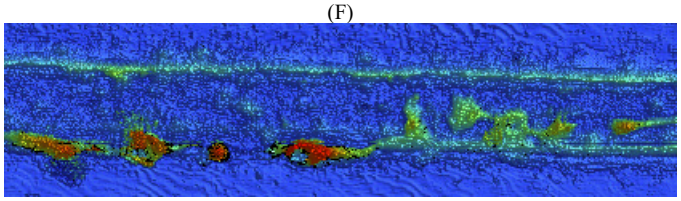

(G)

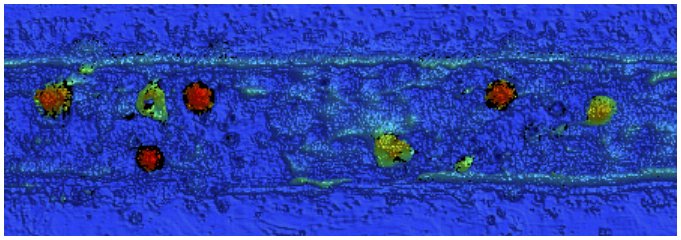

(H)

Fig. 7. Interferometric surface plots of printed conductible lines sintered with different photosintering voltages (A) 1900 V, (B) 1900 V cross-sectional profile at uncracked location, (C) 1900 V cross-sectional profile at cracked location, (D) 2000 V, (E) 2100 V, (F) 2200 V, (G) 2300 V, and (H) 2400 V

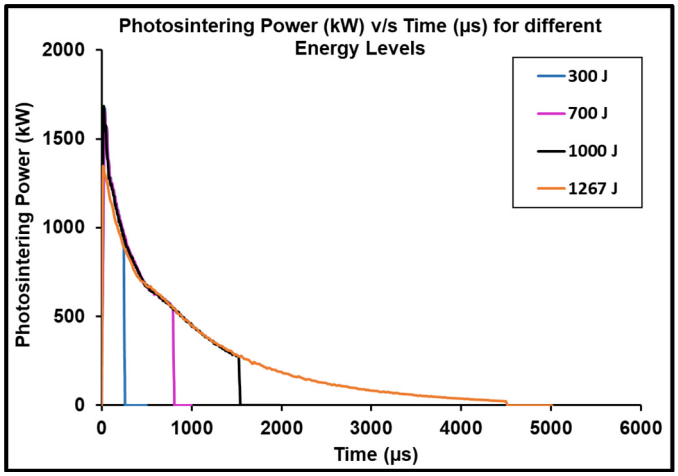

Fig. 8. Photosintering power v/s time for different photosintering flash energies

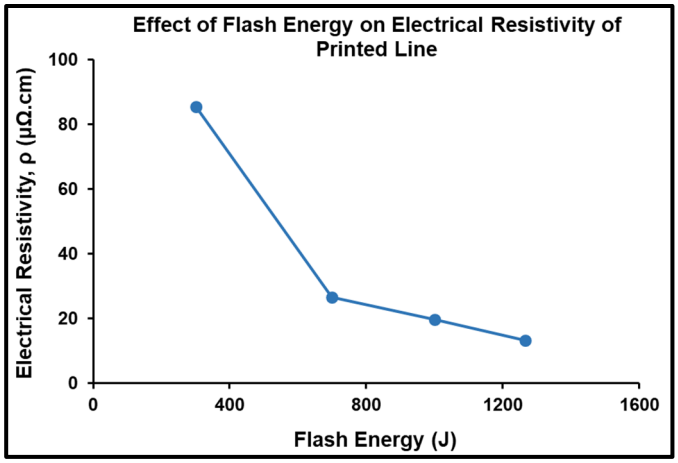

Fig. 9. Effect of photosintering flash energy on electrical resistivity of printed conductive lines

Fig. 9 and Fig. 10 show the plots of electrical resistivity and shear load to failure for different flash energies. With an increase in the flash energy from 300 J to 700 J, a sharp drop in electrical resistivity is seen and the value of the resistivity remains constant as the flash energy is increased from 700 J to 1267 J. In contrast, the shear load to failure sees a sharp increase when the flash energy increases from 300 J to 700 J and later remains constant as the energy is increased from 700 J to 1267 J. This behavior can be attributed to the fact that at lower flash energies, the conductible line is not sintered well enough which leads to a high resistivity and low shear load to failure. This can be validated upon seeing the optical images (Fig. 11), which

shows that the trace sintered with 300 J is much darker in color than the others indicating the presence of unevaporated ink solvent in the trace.

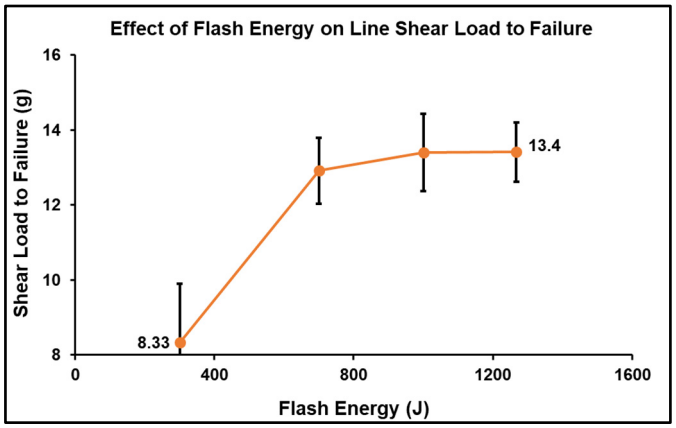

Fig. 10. Effect of photosintering flash energy on shear load to failure of printed conductive lines

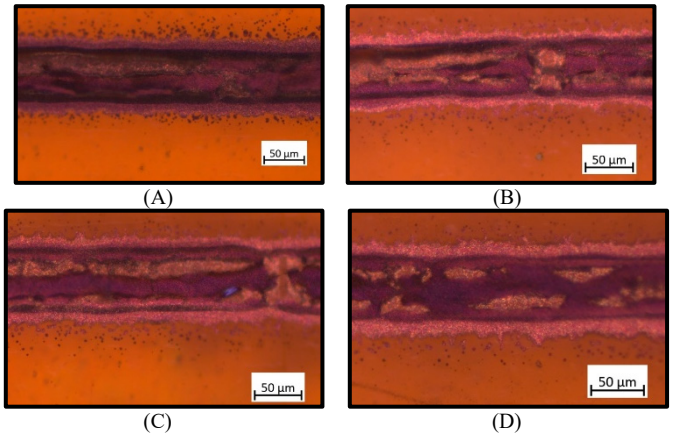

(A) (B) (C) (D)

Fig. 11. Optical images of printed conductible lines sintered with different photosintering flash energies (A) 300 J, (B) 700 J, (C) 1000 J, (D) 1267 J

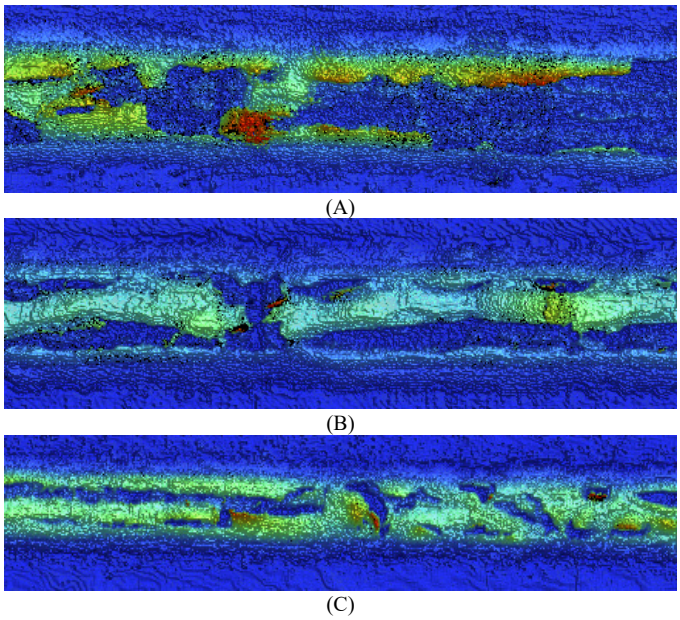

(A) (B) (C)

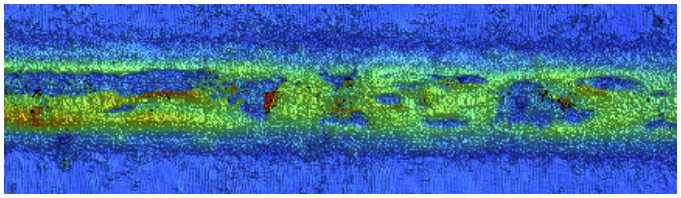

(D)

Fig. 12. Interferometric surface plots of printed conductible lines sintered with different photosintering flash energies (A) 300 J, (B) 700 J, (C) 1000 J, (D) 1267 J

The plots of photosintering power (kW) v/s time are the same for varying the burst frequency and no. of bursts because both the operating voltage and the flash energy is kept constant while varying these other parameters. Fig. 13 and Fig. 14 show the plots of electrical resistivity and shear load to failure for different burst frequencies ranging from 0.5 Hz to 0.125 Hz. Variation of the burst frequency does not seem to have any significant effect on the line resistivity and the shear load to failure as seen in these plots. Also, the optical microscopic images (Fig. 15) and the white light interferometric scans (Fig. 16) are similar in nature and do not show any stark differences. Thus, the rest durations during flashes do not seem to have an effect on the electrical and mechanical properties of the printed conductible line.

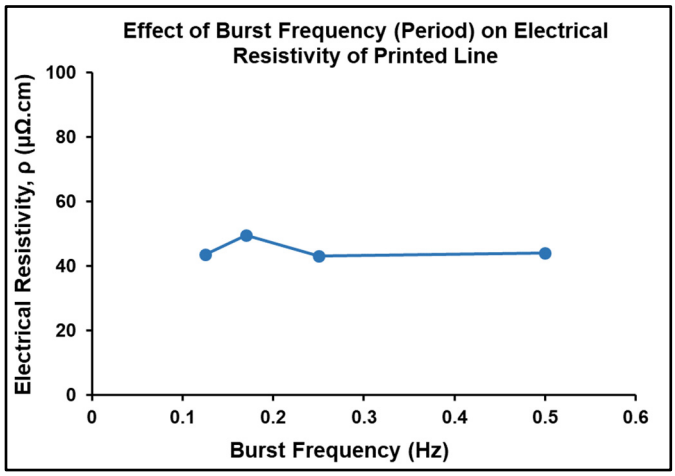

Fig. 13. Effect of photosintering burst frequency on electrical resistivity of printed conductive lines

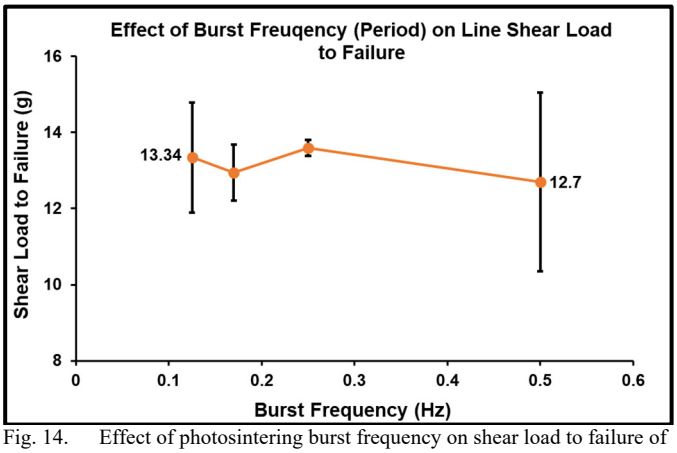

Fig. 14. Effect of photosintering burst frequency on shear load to failure of printed conductive lines

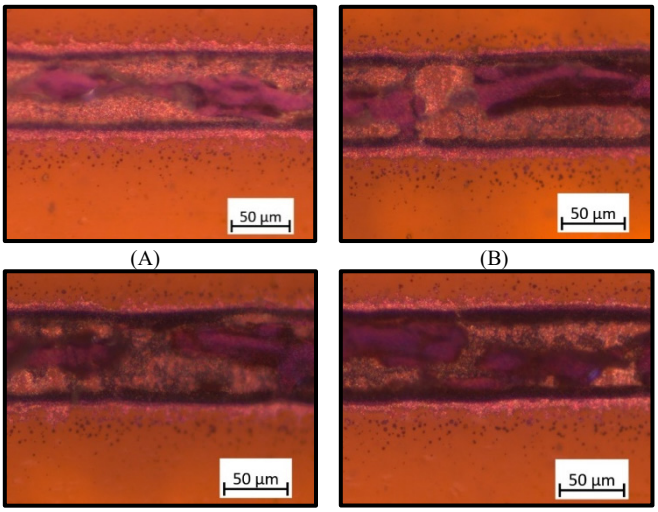

(A) (B) (C) (D)

Fig. 15. Optical images of printed conductible lines sintered with different photosintering burst frequencies (A) 0.5 Hz, (B) 0.25 Hz, (C) 0.17 Hz, (D) 0.125 Hz

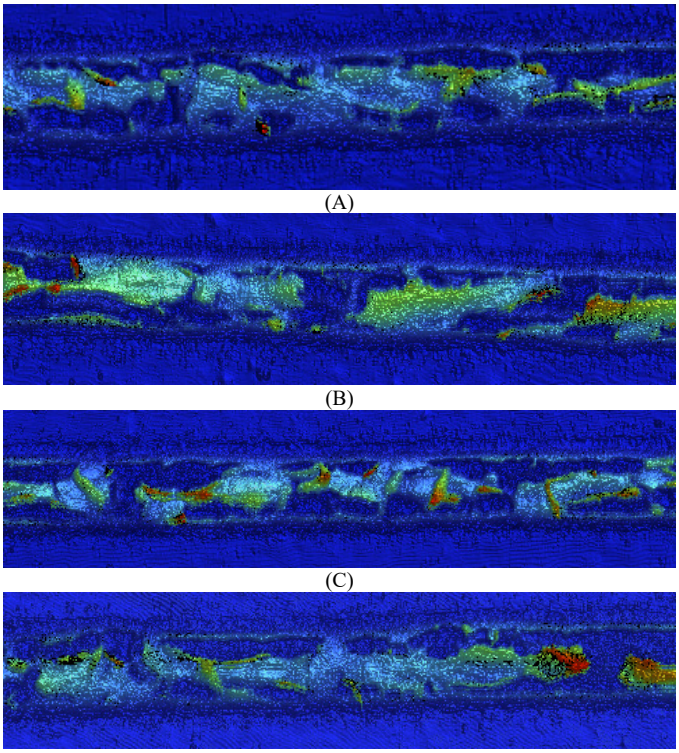

(A) (B) (C) (D)

Fig. 16. Interferometric surface plots of printed conductible lines sintered with different photosintering burst frequencies (A) 0.5 Hz, (B) 0.25 Hz, (C) 0.17 Hz, (D) 0.125 Hz

Fig. 17 and Fig. 18 show the plots of electrical resistivity and shear load to failure for different number of photonic bursts ranging from 1 to 10. An increase in the burst number leads to a linear increase in the electrical resistivity. Also, the shear load to failure first increases until 5 bursts after which it reduces.

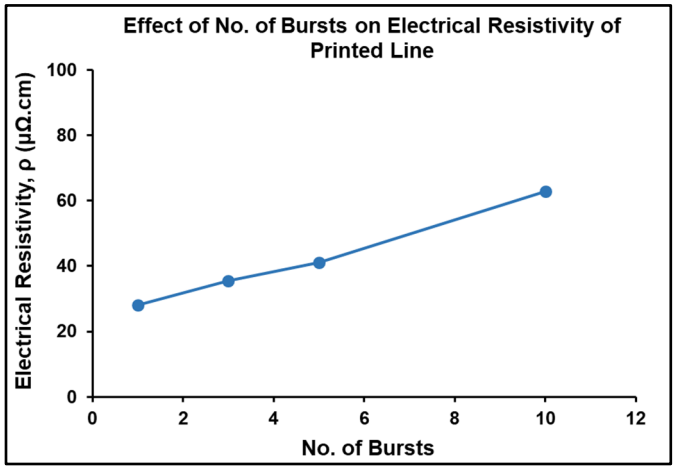

Fig. 17. Effect of number of flashes (bursts) on electrical resistivity of printed conductive lines

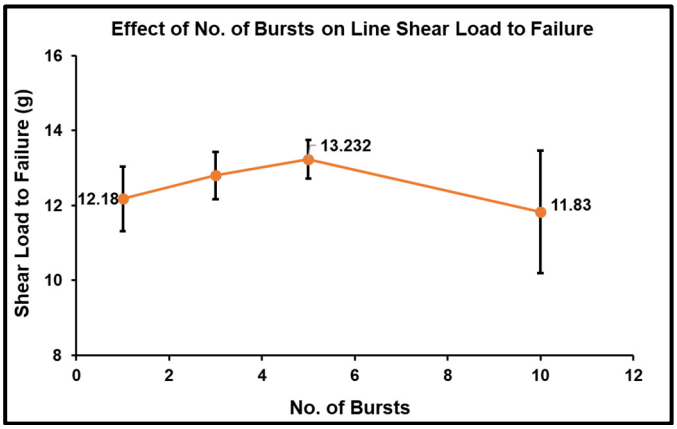

Fig. 18. Effect of number of flashes (bursts) on shear load to failure of printed conductive lines

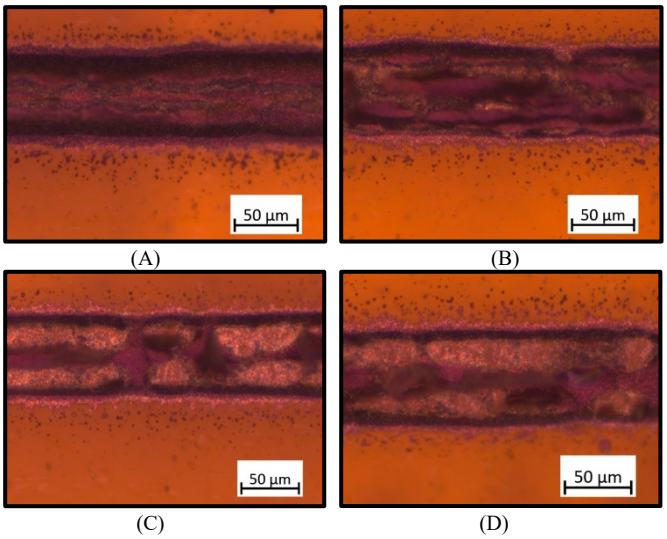

(A) (B) (C) (D)

Fig. 19. Optical images of printed conductible lines sintered with different number of bursts (A) 1 flash, (B) 3 flashes, (C) 5 flashes, and (D) 10 flashes

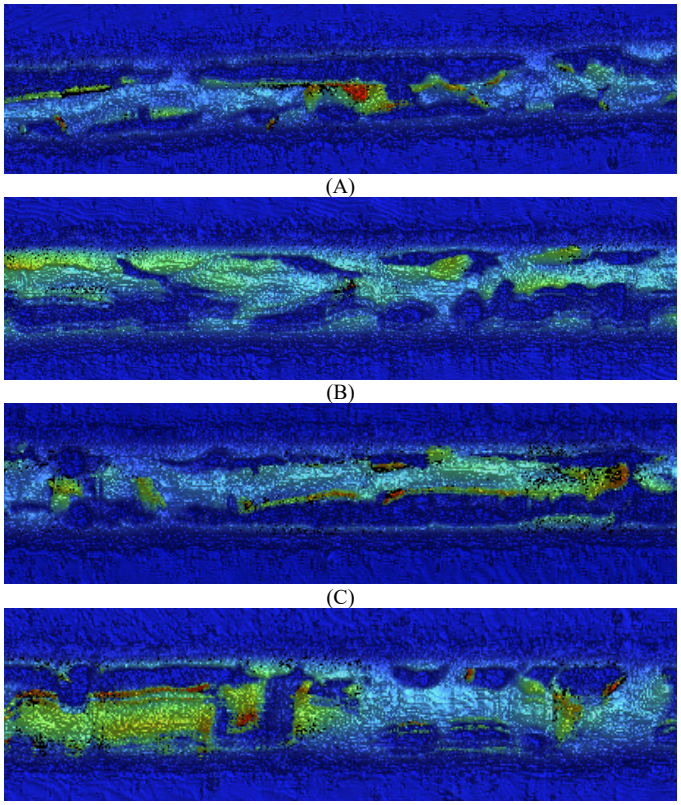

(A) (B) (C) (D)

Fig. 20. Interferometric surface plots of printed conductible lines sintered with different photosintering burst frequencies (A) 1 flash, (B) 3 flashes, (C) 5 flashes, and (D) 10 flashes

B. Effect of oven pre-drying on the electrical and mechanical properties of conductible lines

This section discusses the effect of pre-drying the printed conductible traces in an oven prior to subjecting them to the photosintering process. As mentioned earlier, the samples were affixed on a glass sheet and were placed inside the thermal oven for varying time durations of 5, 15 and 25 minutes at different oven temperatures ranging from 50°C to 80°C. After pre-drying all the traces were sintered at a uniform sintering condition: operating voltage = 2100 V, flash energy = 1000 J, number of bursts = 5, and burst frequency = 0.17 Hz.

Fig. 21 and Fig. 22 show the variation of the electrical resistivity and shear load to failure, respectively, of the oven pre-dried conductive traces and also compares those values with that of the non-pre-dried traces indicated by the black dashed line. As can be seen from Fig. 21, the oven pre-dried samples at 50°C and 65°C show similar resistivity as compared to the non-pre-dried sample for all time durations. However, the sample pre-dried at 80°C has lower resistivity as compared to the non-pre-dried sample especially when the pre-drying is conducted for longer durations of 15 or 25 minutes. The shear load to failure as seen in Fig. 22 shows that all the oven pre-dried samples have almost the same values as compared to that of the non-pre-dried samples irrespective of the pre-drying temperature and time.

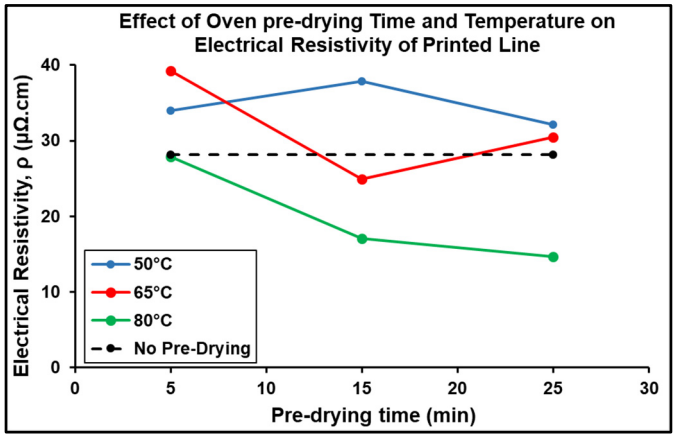

Fig. 21. Effect of oven pre-drying temperature and time on electrical resistivity of printed conductive lines

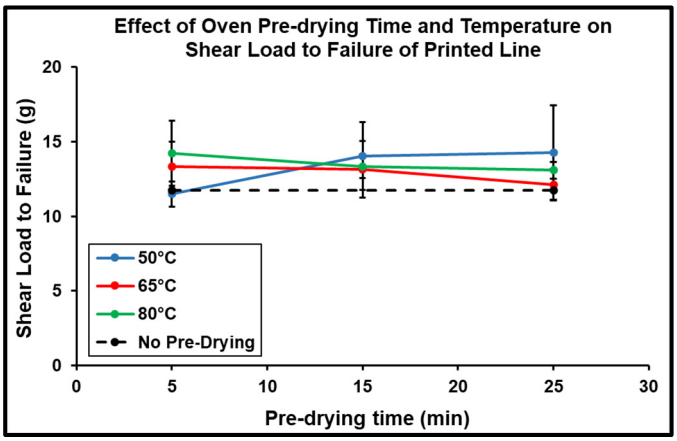

Fig. 22. Effect of oven pre-drying temperature and time on shear load to failure of printed conductive lines

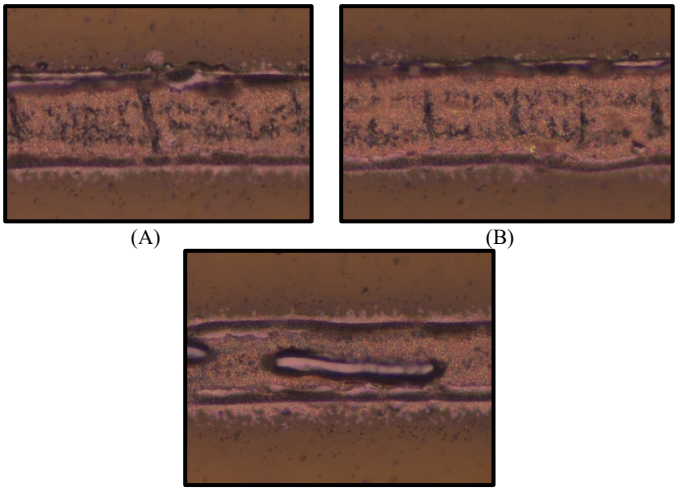

(A) (B) (C)

Fig. 23. Optical images of printed conductible lines oven pre-dried at 50°C for different time periods (A) 5 min, (B) 10 min, and (C) 15 min

Fig. 23 through Fig. 30 show the optical microscopic images and the interferometric surface plots for the oven pre-dried samples as well as the non-pre-dried sample (Fig. 29 and Fig. 30). As can be seen from the interferometric surface plots, there are still cracks present in the line which expose the surface underneath indicating the occurrence of popcorning type failure of these lines which in turn would indicate that the oven pre-

drying conducted has not evaporated the ink solvent completely. However, on comparing Fig. 24, Fig. 26 and Fig. 28 which show the interferometric images of the traces pre-dried at 50℃, 65℃, and 80℃ respectively, it can be seen that the cracks in the line progressively reduce as the pre-drying temperature increases. Moreover, in Fig. 28, as the pre-drying time duration increases, the cracks in the line reduce which also corresponds to the drop in electrical resistivity. Thus, successful pre-drying of the line improves line quality as well as its electrical resistivity.

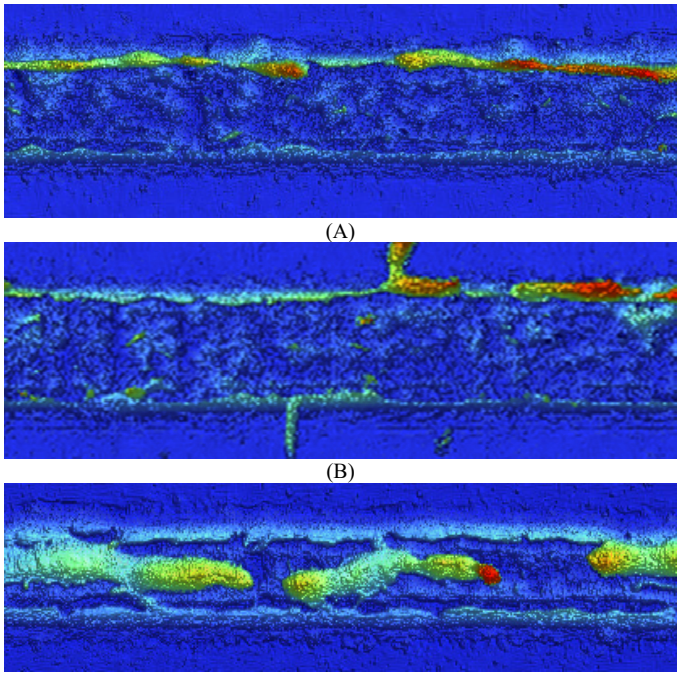

(A)

(B)

(C)

Fig. 24. Interferometric surface plots of printed conductible lines oven pre-dried at 50°C for different time periods (A) 5 min, (B) 10 min, and (C) 15 min

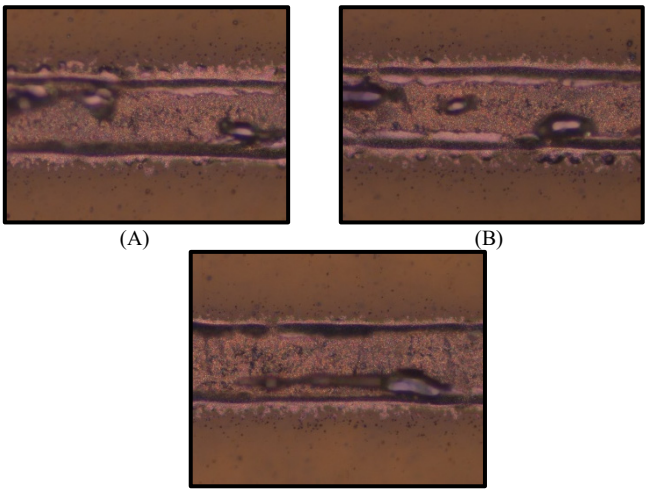

(A) (B)

(C)

Fig. 25. Optical images of printed conductible lines oven pre-dried at 65°C for different time periods (A) 5 min, (B) 10 min, and (C) 15 min

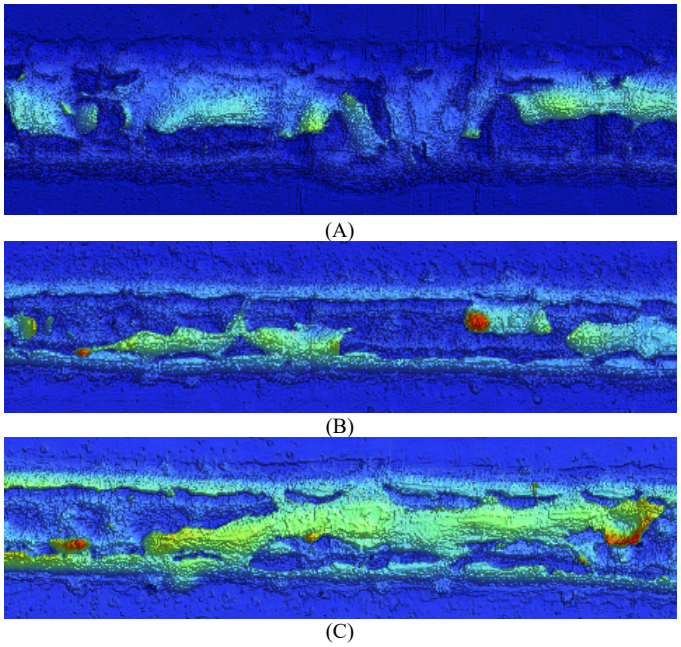

(A)

(B)

(C)

Fig. 26. Interferometric surface plots of printed conductible lines oven pre-dried at 65°C for different time periods (A) 5 min, (B) 10 min, and (C) 15 min

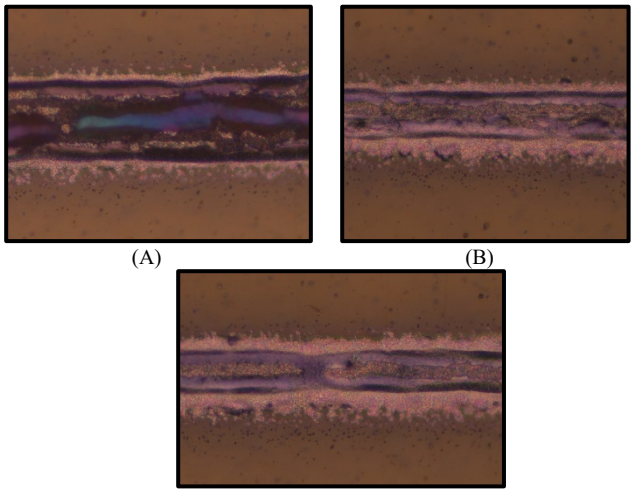

(A) (B)

(C)

Fig. 27. Optical images of printed conductible lines oven pre-dried at 80°C for different time periods (A) 5 min, (B) 10 min, and (C) 15 min

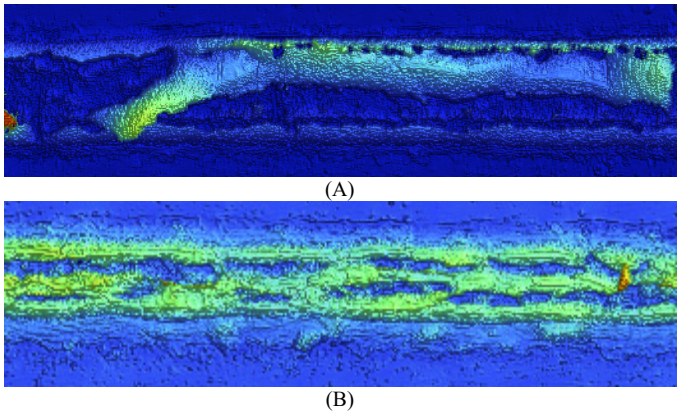

(A)

(B)

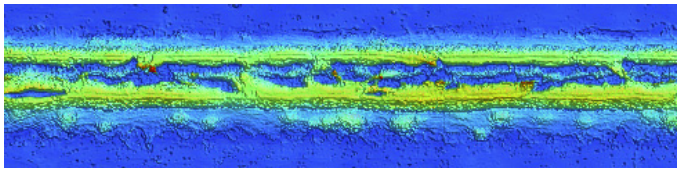

(C)

Fig. 28. Interferometric surface plots of printed conductible lines oven pre-dried at 80°C for different time periods (A) 5 min, (B) 10 min, and (C) 15 min

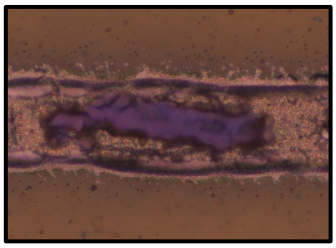

Fig. 29. Optical image of printed conductible line sintered without oven pre-drying

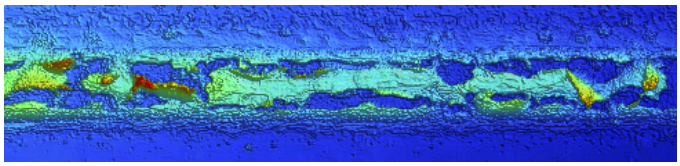

Fig. 30. Interferometric surface plot of printed conductible line sintered without oven pre-drying

C. Effect of platen pre-drying on the electrical and mechanical properties of conductible lines

This section discusses the effect of pre-drying the printed conductible traces on the AJP platen itself prior to subjecting them to the photosintering process. As mentioned earlier, the printing was conducted at an elevated platen temperature and the samples were kept on the platen for total time durations of 5, 15 and 25 minutes at different platen temperatures ranging from 50°C to 80°C. After pre-drying all the traces were sintered at a uniform sintering condition: operating voltage = 2100 V, flash energy = 1000 J, number of bursts = 5, and burst frequency = 0.17 Hz.

Fig. 31 and Fig. 32 show the variation of the electrical resistivity and shear load to failure, respectively, of the platen pre-dried conductive traces and also compares those values with that of the non-pre-dried traces indicated by the black dashed line. As can be seen from Fig. 21, the platen pre-dried samples at 50°C show similar resistivity as compared to the non-pre-dried sample for all time durations. However, the samples pre-dried at 65°C and 80°C has lower resistivity as compared to the non-pre-dried sample for all the time durations. The shear load to failure as seen in Fig. 22 shows that all the platen pre-dried samples have almost the same values as compared to that of the non-pre-dried samples irrespective of the pre-drying temperature and time

Fig. 33 through Fig. 38 show the optical microscopic images and the interferometric surface plots for the platen pre-dried samples. As can be seen from the interferometric surface plots, the samples pre-dried at 50°C show less cracks than the ones which are pre-dried at higher temperatures, especially for the 5 minutes pre-drying case. But apart from that, the cracks are significantly lesser in platen pre-dried samples as compared to oven pre-dried ones and non-pre-dried samples. Thus, this would indicate that platen pre-drying successfully evaporates majority of the ink solvent and hence eliminates the cause for the occurrence of popcorning failure. Furthermore, the difference between the results for platen pre-dried and oven pre-dried samples which are pre-dried at the same temperature and time can be attributed to the fact that the sample might be taking a longer time to reach the set temperature in the oven pre-dried case as it is affixed on a glass sheet and then placed in an oven, whereas in the case of platen pre-drying, the sample is in direct contact with the heated surface which might lead to the solvent being evaporated faster.

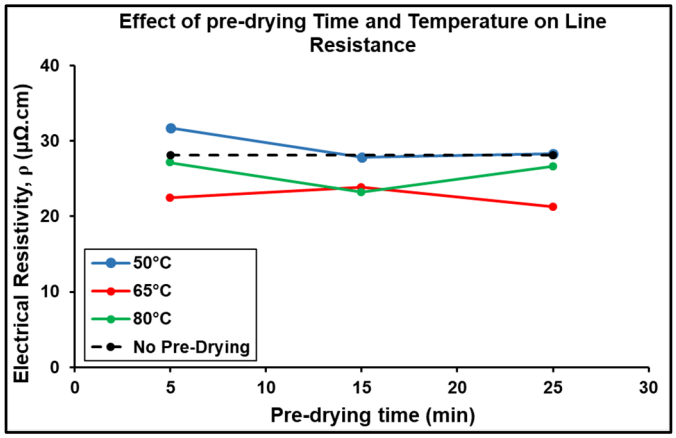

Fig. 31. Effect of platen pre-drying temperature and time on electrical resistivity of printed conductive lines

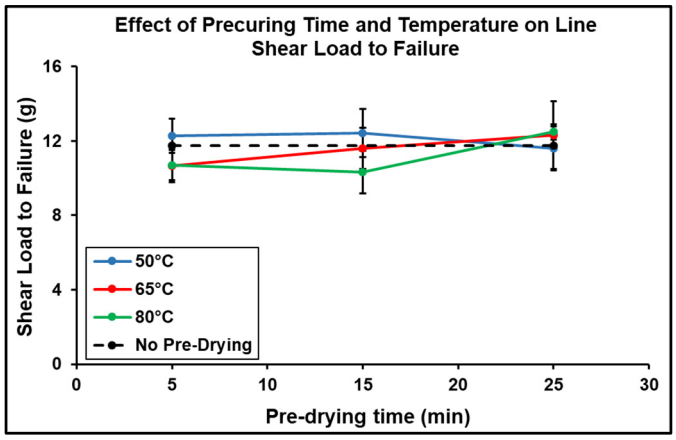

Fig. 32. Effect of oven pre-drying temperature and time on shear load to failure of printed conductive lines

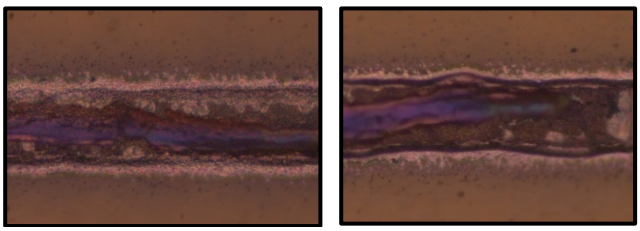

(A) (B)

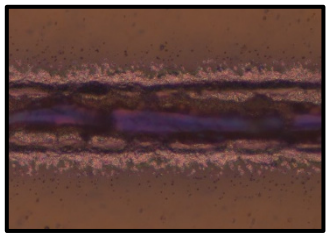

(C)

Fig. 33. Optical images of printed conductible lines platen pre-dried at 50°C for different time periods (A) 5 min, (B) 10 min, and (C) 15 min

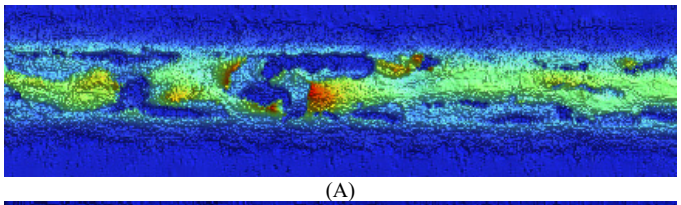

(A)

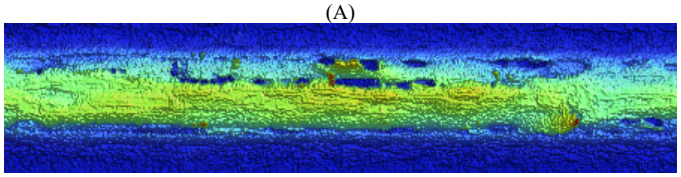

(B)

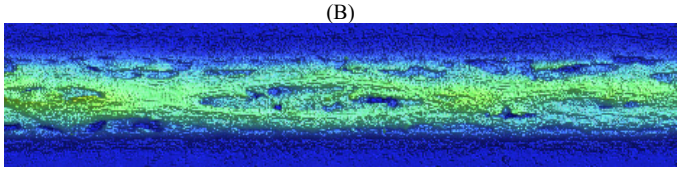

(C)

Fig. 34. Interferometric surface plots of printed conductible lines platen pre-dried at 50°C for different time periods (A) 5 min, (B) 10 min, and (C) 15 min

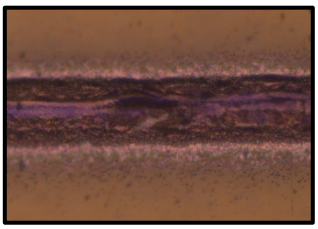

(A)

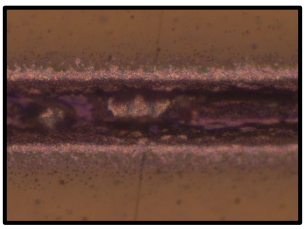

(B)

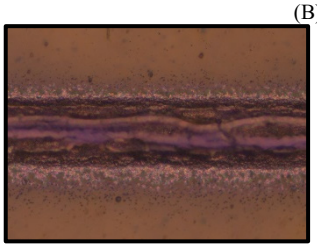

(C)

Fig. 35. Optical images of printed conductible lines platen pre-dried at 65°C for different time periods (A) 5 min, (B) 10 min, and (C) 15 min

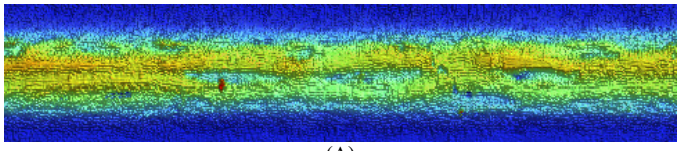

(A)

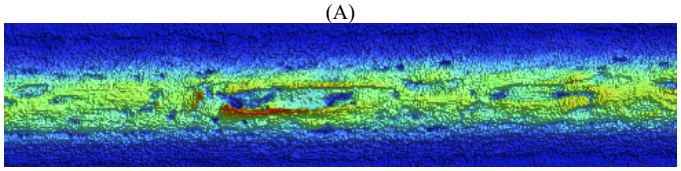

(B)

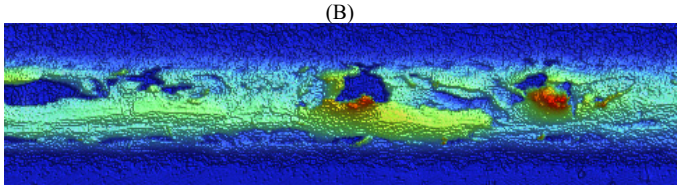

(C)

Fig. 36. Interferometric surface plots of printed conductible lines platen pre-dried at 65°C for different time periods (A) 5 min, (B) 10 min, and (C) 15 min

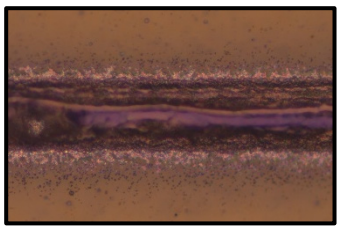

(A)

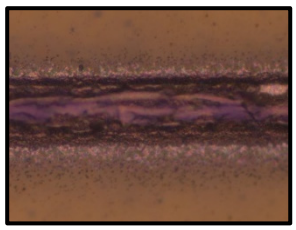

(B)

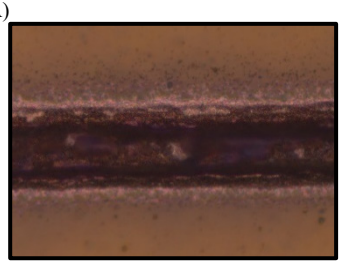

(C)

Fig. 37. Optical images of printed conductible lines platen pre-dried at 80°C for different time periods (A) 5 min, (B) 10 min, and (C) 15 min

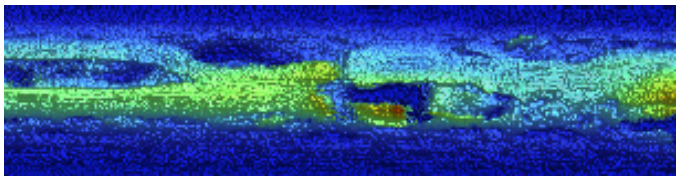

(A)

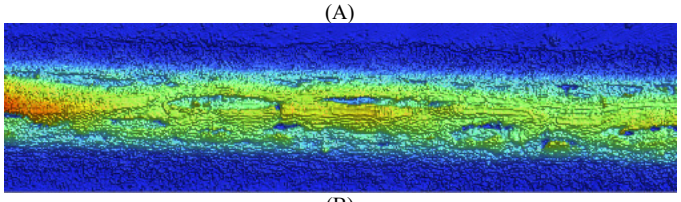

(B)

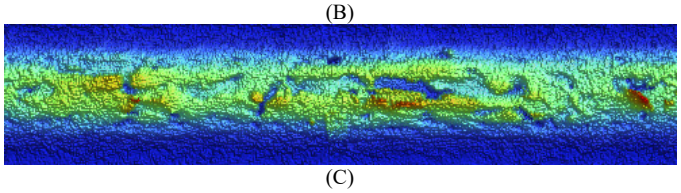

(C)

Fig. 38. Interferometric surface plots of printed conductible lines platen pre-dried at 80°C for different time periods (A) 5 min, (B) 10 min, and (C) 15 min

IV. Summary and Conclusions

In this study, an investigation of photosintering process parameters for sintering a copper conductible ink using Aerosol Jet Printing technology has been conducted. The observations indicate the photosintering voltage, flash energy and number of flashes seem to have a significant effect on the electrical resisticity and shear load to failure values of the printed lines, whereas the burst frequency does not seem to have an effect on these properties. The effect of the variation in these parameters

on the print quality has been demonstrated using optical images and white light interferometric scans. Furthermore, pre-drying of the samples prior to photosintering has been conducted so as to evaporate the ink solvent successfully so as to avoid popcorning failure of the printed traces. Parameters such as the pre-drying temperature and time have been varied to see their effect on the line electrical and mechanical properties. The observed results indicate that the platen pre-drying process is more effective than oven pre-drying as it pre-dries the sample successfully and the process gets completed on the AJP platen itself. A pre-drying temperature of over 65°C and time of over 15 minutes achieves a lower electrical resistivity as compared to the non-pre-dried samples. However, pre-drying does not seem to have an effect on the shear load to failure of the printed line as compared to the non-pre-dried sample.

ACKNOWLEDGEMENTS

The project was sponsored by the NASA Marshall Space Flight Center at the NSF-CAVE3 Electronics Research Center at Auburn University.

REFERENCES

[1] M. Sullivan, "Printed Electronics: Global Markets to 2020," *BCC Research,* 2018.

[2] J. Hoey, A. Lutfurakhmanov, D. Schulz, and I. Akhatov, "A Review on Aerosol-Based Direct-Write and Its Applications for Microelectronics," J. Nanotechnol., vol. 2012, Article ID 324380, 22 pages, 2012.

[3] N.J. Wilkinson, M.A.A. Smith, R.W. Kay, R.A. Harris, "A review of aerosol jet printing—a non-traditional hybrid process for micro-manufacturing," Int. J. Adv. Manuf. Technol., vol. 105, no. 11, pp. 4599-4619, May 2019.

[4] F. Cai, S. Pavlidis, J. Papapolymerou, Y.H. Chang, K. Wang *et al.*, "Aerosol jet printing for 3-D multilayer passive microwave circuitry," 2014 44th European Microwave Conference, pp. 512-515, 2014.

[5] W. Verheecke, M. Van Dyck, F. Vogeler, A. Voet, H. Valkenaers, "Optimizing aerosol jet® printing of silver interconnections on polyimide film for embedded electronics applications," 2012.

[6] A. Mahajan, C.D. Frisbie, L.F. Francis, "Optimization of Aerosol Jet Printing for High-Resolution, High-Aspect Ratio Silver Lines" ACS Appl. Mater. Interfaces, vol. 5, no. 11, pp. 4856-64, May 2013.

[7] E.B. Secor, "Principles of aerosol jet printing," Flex. Print., vol. 3, no. 3, 2018.

[8] P. Lall, K. Goyal, B. Leever and S. Miller, "Factors Influencing the Line Consistency of Commonly Used Geometries for Additively Printed Electronics," 18th IEEE ITherm, pp. 863-869, 2019.

[9] P. Lall, A. Abrol, N. Kothari, B. Leever, S. Miller, "Process Capability of Aerosol-Jet Additive Processes for Long-Runs up to 10-Hours," Proceedings of the ASME 2019 InterPACK, 2019.

[10] M.K. Rahman, Z. Lu, K. Kwon, "Green laser sintering of copper oxide (CuO) nano particle (NP) film to form Cu conductive lines," AIP Advances, vol. 8, no. 9, September 2018.

[11] M.S. Rager, T. Aytug, G.M. Veith, P. Joshi, "Low-thermal-budget, photonic processing of highly conductive Cu interconnects based on CuO nanoinks: potential for flexible printed electronics," ACS Appl. Mater. Interfaces, vol. 8, no. 3, pp. 2441-2448, December 2015.

[12] H. Kang, E. Sowade, R.R. Baumann, "Direct intense pulsed light sintering of inkjet-printed copper oxide layers with six milliseconds," ACS Appl. Mater. Interfaces, vol. 6, no. 3, pp. 1682-1687, January 2014.

[13] W. Chung, Y. Lai, T. Yonezawa, Y. Liao, "Sintering copper nanoparticles with photonic additive for printed conductive patterns by intense pulsed light," Nanomaterials (Basel.), vol. 9, no. 8, July 2019.

[14] H. Hwang, K. Oh, H. Kim, "All-photonic drying and sintering process via flash white light combined with deep-UV and near-infrared irradiation for highly conductive copper nano-ink," Sci. Rep., vol. 6, article no. 19696, January 2016.